Continuum Mech. Thermodyn. (2020) 32:1037–1055
https://doi.org/10.1007/s00161-019-00809-8

ORIGINAL ARTICLE

Jan-Michel C. Farias · Laurent Stainier · Eduardo Alberto Fancello

A variational framework for the modeling of glassy polymers under finite strains

Received: 13 February 2019 / Accepted: 30 June 2019 / Published online: 11 July 2019

Abstract In this paper, a viscoelastic model able to capture important mechanical features of a wide class of glassy polymers is presented. Among them, the ability of reproducing the highly nonlinear rate-dependent stress response and the post-yield strain softening phenomenon. The simplicity of the proposition allows to recover the same mathematical structure of classical constitutive approaches, well suited for the use of implicit finite element codes. To this aim, the *flow resistance* concept, elsewhere known as *shear strength*, is reframed as a state variable of an accumulated strain measure. Three alternative expressions for this function are presented. The model is cast within a variational framework in which consistent constitutive updates are obtained by a minimization procedure. Convenient choices for the conservative and dissipative potentials reduce the local constitutive problem to the solution of a single nonlinear scalar equation, emulating the simplest case of viscoelastic models. Numerical tests on the constitutive model show excellent agreement with experimental data. Finally, a 3D simulation of a standard specimen with heterogeneous material properties illustrates the ability of the present proposition to be implemented in implicit finite element codes.

Keywords Glassy polymers · Variational principles · Viscoelasticity · Finite strain

1 Introduction

Products made of polymers are undoubtedly in our daily routine. These products can exhibit complex shapes and a variety of optical characteristics, a fact that reveals how versatile polymers can be. Further than aesthetics purposes, polymers are being employed to fulfill other needs, such as structural, performance or biocompatibility requirements in biomedical applications [1–4].

Among their wide variety of compositions, amorphous glassy polymers deserve special attention due to their widespread applicability and manufacturing flexibility. Constitutive modeling of polymers depends on the improvement in experimental techniques and numerical methods for predicting their response regarding non-monotonic and coupled loads. Glassy polymers show a significant change of properties when close to the glassy transition. This transition is associated with polymeric mobility, and it is frequently asserted that previously highly constrained chains start exhibiting important rotational and translational movements beyond the glassy transition. Concerning the general behavior, glassy polymers are known to present strong dependency on temperature, strain rate, and pressure [5–13]. In addition, their mechanical properties can vary drastically

J.-M. C. Farias · E. A. Fancello (✉)
Department of Mechanical Engineering, Federal University of Santa Catarina, Florianópolis, SC 88040-900, Brazil
E-mail: eduardo.fancello@ufsc.br

L. Stainier
Research Institute in Civil and Mechanical Engineering (GeM - UMR6183 CNRS/ECN/UN), Ecole Centrale de Nantes, 1 rue de la Nöe, BP 92101, 44321 Nantes, France

according to specific processing conditions [14,15]. Many models can be found in the literature concerning this type of polymers, and interesting surveys are presented by recent papers [16,17]. In the following paragraphs, however, we will focus on those models that are related to the specific contribution of the present manuscript.

Historically, Haward and Thackray [18] attempted to model glassy polymers for a wide range of strains using an unidimensional rheological model. Up to the knowledge of the authors, one of the first extensions to fully tridimensional cases is found in the thesis work of Bagepalli [19] accounting for large deformations, and further developments were carried by Boyce et al. [20].

Since then, a widely used class of models is based on the concept of shear strength evolution, referenced here as flow resistance. This property is named differently across the literature and can also be seen as *athermal shear resistance* [20], *intermolecular resistance to plastic flow* [21], or *microscale athermal shear strength* [22]. This flow resistance property assumes the role of an internal variable and is almost always presented throughout evolution rules in the format of differential equations that have become increasingly complex over time. Examples include the initial BPA model [20], the model of Anand and Gurtin [21], the thermomechanical models of Ames et al. [13] and Srivastava et al. [23], the EBPA model of Holopainen [16], or those of Poulain et al. [22] and Gudimetla and Doghri [17]. When conventional implicit finite element codes are meant to be used, rather complex algebraic coupled equations result from these evolution rules.

Our purpose here is to show that, aided by some simple changes in the flow resistance concept, a variational constitutive framework can be employed for this class of polymers. Over the last two decades, several works concerning variational constitutive updates have been developed. To name a few, Ortiz and Stainier [24] and Radovitzky and Ortiz [25] present a variational framework for dissipative solids, and discuss numerical and mathematical aspects for error estimation and mesh adaptivity. Yang et al. [26] extend an isothermal variational formulation to general dissipative solids considering thermomechanical coupling. Fancello et al. [27] develop a general formulation for finite viscoelasticity based on spectral decomposition. Mosler and Bruhns [28] propose a variational constitutive update based on non-associative plasticity, while Mosler [29] works with finite plasticity and nonlinear kinematic hardening. Kintzel and Mosler [30] use a variational framework to model low cycle fatigue in metals, while El Sayed et al. [31] and Vassoler et al. [32] apply this variational scope to the modeling of biological tissues. Stainier and Ortiz [33] study a coupled thermomechanical variational theory in finite viscoplasticity. Miehe [34] presents a variational constitutive framework for gradient-type dissipative materials. Stainier [35] reports approximation errors when integrating the dissipation potential and develop consistent incremental approximations. Bleier and Mosler [36] discuss the parametrization of the flow rule in the context of variational constitutive updates. Brassart et al. [37,38] employ a variational principle for the homogenization of composites. Brassart and Stainier [39] study the convergence properties of a viscoplastic model. Concerning coupled thermomechanical problems, Bartels et al. [40] adopt a variational approach for the study of finite strain plasticity and the temperature increase during plastic deformation, while Junker and Hackl [41] derive a model for thermomechanically coupled phase transformations in polycrystalline shape memory alloys.

As illustrated by the works listed above, this thermodynamically consistent variational framework allows the inclusion of a variety of dissipative mechanisms in a clear and systematic mathematical setting. In particular, when applied to the current constitutive model, the isothermal formulation of [24] yields one single scalar equation to be numerically solved.

The paper is organized as follows. Section 2 concerns the introduction of some basic kinematic assumptions followed by the thermodynamic potentials of the current formulation. Section 3 sets the developed model in a variational framework where all the equations are formally obtained. The key aspects regarding the flow resistance variable are then introduced in Sect. 5 and the connections between existing models are made. Section 6 provides some numerical examples of the model through comparison against experimental data and assessment of a FEM test case.

2 Constitutive modeling

2.1 Kinematics

The kinematic variables adopted in the current visco-hyperelastic model follow assumptions commonly used in the literature. The multiplicative decomposition defined by Lee [42] is employed to split the deformation gradient $\boldsymbol{F}$ into elastic $\boldsymbol{F}^{\mathrm{e}}$ and inelastic $\boldsymbol{F}^{\mathrm{p}}$ contributions

$$\boldsymbol{F} = \boldsymbol{F}^{\mathrm{e}}\boldsymbol{F}^{\mathrm{p}} \tag{1}$$

In addition, the inelastic flow is assumed to be isochoric ($\det \boldsymbol{F}^{\mathrm{p}} = 1$), and consequently, the inelastic velocity gradient $\boldsymbol{L}^{\mathrm{p}} = \dot{\boldsymbol{F}}^{\mathrm{p}} \left(\boldsymbol{F}^{\mathrm{p}}\right)^{-1}$ is a traceless tensor. The inelastic flow is also assumed to be irrotational, which is expressed by a null inelastic spin $\boldsymbol{W}^{\mathrm{p}}$. Based on this last assumption, the inelastic velocity gradient $\boldsymbol{L}^{\mathrm{p}}$ becomes symmetric and equal to the inelastic stretching tensor $\boldsymbol{D}^{\mathrm{p}}$

$$\boldsymbol{L}^{\mathrm{p}} = \boldsymbol{D}^{\mathrm{p}} + \boldsymbol{W}^{\mathrm{p}}, \quad \boldsymbol{W}^{\mathrm{p}} = \boldsymbol{0} \Rightarrow \dot{\boldsymbol{F}}^{\mathrm{p}} \left(\boldsymbol{F}^{\mathrm{p}}\right)^{-1} = \boldsymbol{D}^{\mathrm{p}} \tag{2}$$

or equivalently

$$\dot{\boldsymbol{F}}^{\mathrm{p}} = \boldsymbol{D}^{\mathrm{p}} \boldsymbol{F}^{\mathrm{p}} \tag{3}$$

which defines an evolution law for the inelastic deformation gradient. This last expression is used as an important link to connect different thermodynamic states when dealing with discrete time steps. It is also assumed that an isochoric deformation gradient $\boldsymbol{F}^{\mathrm{iso}}$ can be obtained directly from the deformation gradient and the Jacobian ($J = \det \boldsymbol{F}$)

$$\boldsymbol{F}^{\mathrm{iso}} = J^{-\frac{1}{3}} \boldsymbol{F} \tag{4}$$

These kinematic assumptions are represented in the rheological model shown in Fig. 1.

2.2 Thermodynamic framework

The major difference among the available models used to describe glassy polymers [16,20,21,43] and the current work relies on thermodynamic aspects. These previous works assume the existence of an internal variable called *flow resistance* whose evolution is controlled by a set of time differential equations solved as part of the constitutive problem. Within the present approach, this mechanical property becomes dependent on another convenient variable.

The thermodynamic state $\mathcal{E}$ of a sufficiently small neighborhood around a material point $\boldsymbol{X}$ is assumed to be uniquely described by the total deformation gradient $\boldsymbol{F}$, and two internal variables; the inelastic deformation gradient $\boldsymbol{F}^{\mathrm{p}}$ and by a scalar quantity r referenced as the *accumulated inelastic strain*:

$$\mathcal{E} = \left\{\boldsymbol{F}, \boldsymbol{F}^{\mathrm{p}}, r\right\} \tag{5}$$

The accumulated inelastic strain is a measure of how much the material has undergone inelastic stretching, up to the current time t. It is formally defined by

$$r = \int_0^t \sqrt{2} \left\| \boldsymbol{D}^{\mathrm{p}} \right\| \mathrm{d}t \tag{6}$$

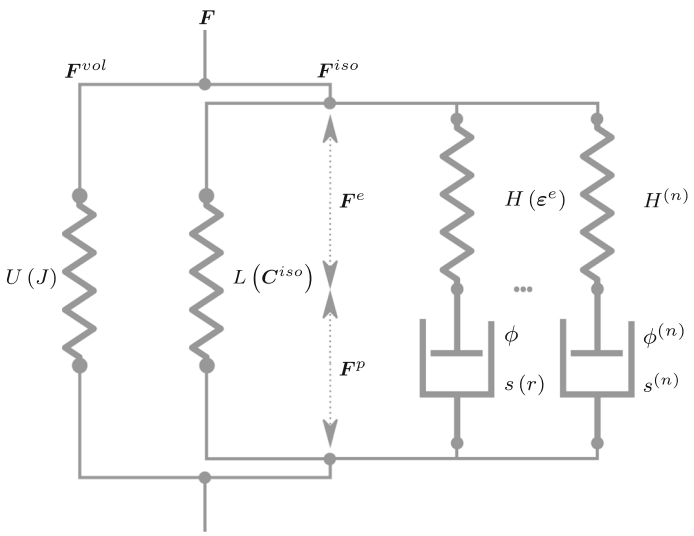

Fig. 1 Schematic representation of the current proposition through the use of a rheological model. Main features are depicted: the energy potentials are represented by springs (Eq. 7); the dissipation potentials are represented by dashpots (Eq. 17); and the explicit use of a state-dependent flow resistance $s\,(r)$ is shown (Eq. 18)

2.2.1 Helmholtz free energy

Following a frequently used approach in the literature, the Helmholtz free energy ψ is split into three potentials

$$\psi\left(\mathcal{E}\right) = U\left(J\right) + L\left(\boldsymbol{C}^{\text{iso}}\right) + H\left(\boldsymbol{\varepsilon}^{\text{e}}\right) \tag{7}$$

Moreover, each potential has its own state dependence by means of specific variables related to the physical behavior each one is meant to model. This separation is classical and provides flexibility for different approaches concerning incompressibility issues [44]. The first term accounts for the accumulated energy based exclusively on the Jacobian measure of volumetric deformation ($J = \det \boldsymbol{F}$), and is for example given by

$$U\left(J\right) = \frac{\kappa}{2}\left(\ln J\right)^2 \tag{8}$$

Polymeric chains may undergo large values of stretching which can eventually make them reach their ultimate extension capabilities. In this case, large quantities of energy would be required to further stretch the chains, rendering at the end a virtual state of locking. Hyperelastic models that are concerned with these phenomena are well represented by the eight-chain model, introduced by Arruda and Boyce [45], or by the model due to Gent [46]. The latter is used here for the potential L in (7)

$$L\left(\boldsymbol{C}^{\text{iso}}\right) = -\frac{\lambda\mu_L}{2}\ln\left[\frac{\lambda + 3 - \text{tr}\left(\boldsymbol{C}^{\text{iso}}\right)}{\lambda}\right] \tag{9}$$

where the isochoric right Cauchy–Green tensor $\boldsymbol{C}^{\text{iso}}$ is expressed by

$$\boldsymbol{C}^{\text{iso}} = \left(\boldsymbol{F}^{\text{iso}}\right)^T \boldsymbol{F}^{\text{iso}} \tag{10}$$

Finally, we consider a quadratic Hencky energy potential H, given by

$$H\left(\boldsymbol{\varepsilon}^{\text{e}}\right) = \mu_H \left\|\text{dev}\left(\boldsymbol{\varepsilon}^{\text{e}}\right)\right\|^2 \tag{11}$$

and dependent on the logarithmic elastic strain $\boldsymbol{\varepsilon}^{\text{e}}$

$$\boldsymbol{\varepsilon}^{\text{e}} = \frac{1}{2}\ln \boldsymbol{C}^{\text{e}}, \quad \boldsymbol{C}^{\text{e}} = \left(\boldsymbol{F}^{\text{e}}\right)^T \boldsymbol{F}^{\text{e}} \tag{12}$$

being $\boldsymbol{C}^{\text{e}}$ the elastic right-Cauchy tensor. Intuitively, Fig. 1 depicts these energy potentials as springs in the rheological model. One can notice the possibility of appending multiple Hencky potentials, which will be clarified in Sect. 4. This is part of a strategy for improving the description of unloading conditions seen in some polymers.

2.2.2 Dissipation potential

From a given state $\mathcal{E}$ (Eq. 5), it remains to define the process $\dot{\mathcal{E}}$

$$\dot{\mathcal{E}} = \left\{\dot{\boldsymbol{F}}, \dot{\boldsymbol{F}}^{\text{p}}, \dot{r}\right\} \tag{13}$$

that drives the current state toward the next one. A process should be understood as a set of differential equations, typically written in a rate format, that completely defines the evolution of the variables within the model. Even though the inelastic deformation gradient $\boldsymbol{F}^{\text{p}}$ and the accumulated inelastic strain r are state variables, their evolution cannot be arbitrarily set. We assume that the evolution of the internal variables depend solely on the current state,

$$\dot{\boldsymbol{F}}^{\text{p}} = \dot{\boldsymbol{F}}^{\text{p}}\left(\mathcal{E}\right) \tag{14}$$

$$\dot{r} = \dot{r}\left(\mathcal{E}\right) \tag{15}$$

and thus they define the internal process $\dot{\mathcal{E}}_i$

$$\dot{\mathcal{E}}_i = \left\{\dot{\boldsymbol{F}}^{\text{p}}, \dot{r}\right\} \tag{16}$$

If the state is known, then by the aid of Eq. (3), it is sufficient to propose an expression (or *flow rule*) for the inelastic stretching $\boldsymbol{D}^{\mathrm{p}}$ in order to completely define $\dot{\boldsymbol{F}}^{\mathrm{p}}$.

Dissipative mechanisms considered are those of slippage and constant re-adaption of polymeric chains. They are accounted by means of a dissipative potential ϕ dependent on the current state and on the rates of internal variables. A power-law-type expression is convenient for the present case:

$$\phi\left(\dot{r}; r\right) = \begin{cases} \dot{r}_0 \frac{s(r)}{m+1} \left(\frac{\dot{r}}{\dot{r}_0}\right)^{m+1} & \dot{r} \geq 0 \\ \infty & \dot{r} < 0 \end{cases} \tag{17}$$

It is possible to see that ϕ in (Eq. 17) is a state-dependent dissipative potential in the sense that, in addition to its dependence on the rate $\dot{r}$, it also depends parametrically on the state through the state equation $s = s(r)$. This kind of description is thermodynamically consistent in the continuous time formulation and compatible with thermodynamic theories such as that of Ziegler [47], for example. Moreover, numerical consequences of this type of potential in the discrete time formulation were thoroughly discussed in [38,39].

The special feature to be highlighted on the above potential is the adoption of an explicit expression for the flow resistance property (s), one of the most important properties concerning the modeling of glassy polymers.

As mentioned previously, since the seminal ideas of Boyce et al. [20], the flow resistance is taken as an internal variable endowed with evolution rules that became increasingly complex over the years. Examples include the models from Boyce et al. [20], Anand and Gurtin [21], Ames et al. [13], Srivastava et al. [23], Holopainen [16], Poulain et al. [22], Gudimetla and Doghri [17]. Aided by some simple changes, our approach reframes the theoretical perspective on the flow resistance. In the present context, the flow resistance assumes the role of a state variable dependent on the internal variable r

$$s = s\left(r\right) \tag{18}$$

where r is the accumulated inelastic strain (Eq. 6). Once this state equation (Eq. 18) is defined, the current value of s is obtained by a simple evaluation from the current value of r. This perspective allows one to see the flow resistance as a path-independent variable, in the sense that two different thermodynamic processes that lead to the same final accumulated inelastic strain would render the same value of s.

From a numerical point of view, if an implicit finite element approach is adopted, all these previous cited models have in common that the flow resistance and other associated variables are incrementally updated based on the solution of a nonlinear coupled system of equations. Clearly, the dimension and intricacies of this system are influenced by the number of internal variables involved in the solution, the flow resistance being one of them. Alternatively, an explicit finite element formulation seems to be usually employed to circumvent this system, the update algorithm of which becomes straightforward. In what follows, it is shown that the proposed approach is simple enough to be incorporated effortlessly into classical implicit finite element implementations.

As it will be evident, it is possible to obtain the same overall flow resistance behavior from these previous references in a cleaner environment, which offers an alternative strategy for the description of glassy polymers. Examples of such an explicit expression (Eq. 18) and further discussion will be given in Sect. 5 for a better model overview.

2.2.3 Parametrized inelastic stretching

The accumulated inelastic strain r and its rate $\dot{r}$ depend on the inelastic stretching tensor $\boldsymbol{D}^{\mathrm{p}}$ (see Eq. 6). This relationship is conveniently highlighted by a parametrization $\mathcal{P} = \{\dot{r}, \boldsymbol{N}\}$ that decomposes $\boldsymbol{D}^{\mathrm{p}}$ in the scalar $\dot{r} \in \mathbb{R}_+$ and the tensor $\boldsymbol{N}$:

$$\boldsymbol{D}^{\mathrm{p}} = \dot{r}\boldsymbol{N} \tag{19}$$

$$\boldsymbol{N} \in \mathcal{N} = \left\{ \boldsymbol{A} \in Sym \,|\, \mathrm{tr}\boldsymbol{A} = 0 \quad and \quad \|\boldsymbol{A}\| = \frac{1}{\sqrt{2}} \right\} \tag{20}$$

This operation is often referred as an amplitude–direction decomposition, with the stretching magnitude described by $\dot{r}$ and all other tensorial properties held by $\boldsymbol{N}$, thus effectively defining the flow direction. The constraints (20) over $\boldsymbol{N}$, concerning symmetry and traceless conditions, arise from those of the inelastic

velocity gradient $\boldsymbol{L}^{\mathrm{p}}$. The norm of $\boldsymbol{N}$ comes directly as a consequence of definitions (Eqs. 6, 19). By doing so, an internal process $\dot{\mathcal{E}}_i = \left\{\dot{\boldsymbol{F}}^{\mathrm{p}}, \dot{r}\right\}$ (Eq. 16) can be directly mapped to the parametrization $\mathcal{P}$ by Eq. (3)

$$\dot{\boldsymbol{F}}^{\mathrm{p}} = \boldsymbol{D}^{\mathrm{p}}\boldsymbol{F}^{\mathrm{p}} = \dot{r}\boldsymbol{N}\boldsymbol{F}^{\mathrm{p}} \tag{21}$$

This alternative approach, with the amplitude–direction assumption, is stated as the parametrized constitutive problem [24]. This parametrization ($\mathcal{P}$) provides some operational conveniences and becomes a mean to better understand and distinguish different aspects of the inelastic flow.

3 Variational constitutive updates

Variational constitutive updates correspond to a class of methods in which the constitutive updates for a given time discretization are based on variational principles. That is, the rules employed to update a thermodynamic state to the next one originate from an extremization process. Over the field of inelastic materials, this approach can be linked to the works of Hill [48], Ceradini [49], Maier [50], Capurso and Maier [51], Pereira and Feijoo [52], Martin et al. [53], to name a few, with emphasis on elastoplasticity. The technique employed here is based on [24]. After discussing a sequence of examples, these authors demonstrate a variational principle with thermodynamic foundation to describe general dissipative materials, especially suited to numerical incremental procedures. As a direct consequence, they also highlight that this variational structure can be exploited for error estimates and mesh adaption techniques (see [24,25,54,55]).

3.1 Continuous time description

To demonstrate the variational nature of the constitutive problem, we focus primarily on a continuous time description. All required equations are shown to be obtained from the stationarity conditions of a potential. It can be formally done by the statement:

Variational Principle - Given a state $\mathcal{E} = \{\boldsymbol{F}, \boldsymbol{F}^{\mathrm{p}}, r\}$ (Eq. 5) and the total deformation gradient rate $\dot{\boldsymbol{F}}$, the process described by the parametrization $\mathcal{P} = \{\dot{r}, \boldsymbol{N}\}$ that minimizes the functional $\dot{\Psi}$, among all admissible internal processes $\dot{\mathcal{E}}_i = \left\{\dot{\boldsymbol{F}}^{\mathrm{p}}, \dot{r}\right\}$ (Eq. 16), corresponds to the effective one

$$\inf_{\substack{\dot{r} \in \mathbb{R}_+ \\ \boldsymbol{N} \in \mathcal{N}}} \dot{\Psi} = \frac{\mathrm{d}}{\mathrm{d}t}\psi\left(\mathcal{E}\right) + \phi\left(\dot{\mathcal{E}}; \mathcal{E}\right) \tag{22}$$

The functional $\dot{\Psi}$ is built directly from the Helmholtz free energy ψ (Eq. 7) and the dissipation potential ϕ (Eq. 17). From the optimality conditions of the problem (22), one can recover the desired flow equation, expressed in terms of the direction

$$\boldsymbol{N} = \frac{1}{\sqrt{2}} \frac{\mathrm{sym}_0\left(\boldsymbol{M}^{\mathrm{e}}\right)}{\left\|\mathrm{sym}_0\left(\boldsymbol{M}^{\mathrm{e}}\right)\right\|} \tag{23}$$

and the amplitude $\dot{r}$, which satisfies the nonlinear equation

$$-\frac{1}{\sqrt{2}}\left\|\mathrm{sym}_0\left(\boldsymbol{M}^{\mathrm{e}}\right)\right\| + s\left(r\right)\left(\frac{\dot{r}}{\dot{r}_0}\right)^m = 0 \tag{24}$$

where $\boldsymbol{M}^{\mathrm{e}}$ is a stress measure given by

$$\boldsymbol{M}^{\mathrm{e}} = 2\boldsymbol{C}^{\mathrm{e}}\frac{\partial \psi}{\partial \boldsymbol{C}^{\mathrm{e}}} \tag{25}$$

The symbol $\mathrm{sym}_0\left(\cdot\right)$ stands for the symmetric–deviatoric operator.

Finally, and following the variational framework [24], the first Piola–Kirchhoff stress tensor is obtained directly from an effective potential $\dot{\Psi}_{\mathrm{eff}}$, which gathers all the minima from the above variational principle as a function of $\dot{\boldsymbol{F}}$

$$\boldsymbol{P} = \frac{\partial \dot{\Psi}_{\mathrm{eff}}}{\partial \dot{\boldsymbol{F}}}, \quad \dot{\Psi}_{\mathrm{eff}}\left(\dot{\boldsymbol{F}}\right) = \inf_{\substack{\dot{r} \in \mathbb{R}_+ \\ \boldsymbol{N} \in \mathcal{N}}} \frac{\mathrm{d}}{\mathrm{d}t}\psi\left(\mathcal{E}\right) + \phi\left(\dot{\mathcal{E}}; \mathcal{E}\right) \tag{26}$$

In the particular case of the current viscoelastic model, the first Piola–Kirchhoff is shown to be a state-dependent variable dependent solely on the Helmholtz free energy. As a consequence, the first Piola–Kirchhoff is composed of three stress tensors, each one originated from one of the energetic potentials (Eq. 7)

$$\boldsymbol{P} = \frac{\partial \dot{\Psi}_{\text{eff}}}{\partial \dot{\boldsymbol{F}}} = \frac{\partial \psi}{\partial \boldsymbol{F}} = \frac{\partial U}{\partial \boldsymbol{F}} + \frac{\partial L}{\partial \boldsymbol{F}} + \frac{\partial H}{\partial \boldsymbol{F}} \tag{27}$$

Straightforwardly, the Cauchy stress can be obtained from $\boldsymbol{P}$ through the usual operation

$$\boldsymbol{\sigma} = J^{-1} \boldsymbol{P} \boldsymbol{F}^T \tag{28}$$

3.2 Incremental constitutive update

In order to solve the constitutive problem above, it becomes necessary to appeal for numerical methods. The incremental version of the current constitutive problem is called the *update algorithm*, that is, starting from a thermodynamic state $\mathcal{E}_n$ defined at the time step t_n, the next thermodynamic state $\mathcal{E}_{n+1}$ at time step t_{n+1} is sought. In order to generate such a procedure, the existing rates must be somehow rewritten by their discrete counterparts. The discrete version of $\dot{r}$ becomes $\mathring{r}$ and keeps the same physical meaning as before, relating the states r_{n+1} and r_n by

$$r_{n+1} = r_n + \mathring{r} \Delta t \tag{29}$$

The update of the inelastic deformation gradient $\boldsymbol{F}^{\text{p}}{}_{n+1}$ is conveniently performed by the exponential mapping [56]

$$\boldsymbol{F}^{\text{p}}{}_{n+1} = \text{EXP}\left[\mathring{r} \boldsymbol{N} \Delta t\right] \boldsymbol{F}^{\text{p}}_n \tag{30}$$

since it preserves the isochoric nature of the inelastic flow $\left(\det \boldsymbol{F}^{\text{p}}_{n+1} = \det \boldsymbol{F}^{\text{p}}_n = 1\right)$, once the traceless condition $\text{tr}\boldsymbol{D}^{\text{p}} = 0$ is fulfilled. Calculation of $\mathring{r}$ and $\boldsymbol{N}$ finally comes from the solution of the incremental variational problem below [24]

Incremental Variational Update - Given a state $\mathcal{E}_n = \left\{\boldsymbol{F}_n, \boldsymbol{F}^{\text{p}}_n, r_n\right\}$ at time t_n and the total deformation gradient $\boldsymbol{F}_{n+1}$ at time t_{n+1}, the state $\mathcal{E}_{n+1} = \left\{\boldsymbol{F}_{n+1}, \boldsymbol{F}^{\text{p}}_{n+1}, r_{n+1}\right\}$ at time t_{n+1} described by the parametrization $\mathcal{P} = \left\{\mathring{r}, \boldsymbol{N}\right\}$ that minimizes the incremental potential Ψ_{inc} among all admissible states corresponds to the effective updated state

$$\inf_{\substack{\mathring{r} \in \mathbb{R}_+ \\ \boldsymbol{N} \in \mathcal{N}}} \Psi_{\text{inc}} = \psi\left(\mathcal{E}_{n+1}\right) - \psi\left(\mathcal{E}_n\right) + \Delta t \phi\left(\mathring{\mathcal{E}}; \mathcal{E}_{n+\alpha}\right) \tag{31}$$

Some terms need to be detailed. The symbolism $\mathcal{E}_{n+\alpha}$ stands for an intermediate state at time $t_{n+\alpha} \in \left[t_n, t_{n+1}\right]$, $\alpha \in [0, 1]$, and $\mathring{\mathcal{E}}$ refers to a discrete, or incremental version of a process. On the other hand, the abstract notation $\left(\mathring{\mathcal{E}}; \mathcal{E}_{n+\alpha}\right)$ can be effectively replaced by $(\mathcal{E}_n, \mathcal{E}_{n+1})$ to make clear that only two discrete instants of time are in fact available, and any intermediate state is approximated by an interpolation of these two states.

The optimality condition of Eq. (31) aligned with the convenient choice of a quadratic Hencky type potential (Eq. 11), allows for an analytical expression for the flow direction $\boldsymbol{N}$

$$\boldsymbol{N} = \frac{1}{\sqrt{2}} \frac{\text{dev}\left(\boldsymbol{\varepsilon}^{\text{pre}}_{n+1}\right)}{\left\|\text{dev}\left(\boldsymbol{\varepsilon}^{\text{pre}}_{n+1}\right)\right\|} \tag{32}$$

which depends solely on an elastic predictor state $\mathcal{E}^{\text{pre}}_{n+1} = \left\{\boldsymbol{F}_{n+1}, \boldsymbol{F}^{\text{p}}_n, r_n\right\}$ defined at time t_{n+1}, where

$$\boldsymbol{\varepsilon}^{\text{pre}}_{n+1} = \frac{1}{2} \ln \boldsymbol{C}^{\text{pre}}_{n+1}, \quad \boldsymbol{C}^{\text{pre}}_{n+1} = \left(\boldsymbol{F}^{\text{pre}}_{n+1}\right)^T \boldsymbol{F}^{\text{pre}}_{n+1}, \quad \boldsymbol{F}^{\text{pre}}_{n+1} = \boldsymbol{F}_{n+1} \left(\boldsymbol{F}^{\text{p}}_n\right)^{-1}. \tag{33}$$

Other general expressions for the elastic potential (H) could be employed. The spectral projection used by Fancello et al. [27] would widen the formulation to more general isotropic elastic potentials, such as the Ogden model, also allowing for a semi-analytical solution. Other approaches lead to the solution of a fully coupled

system for both the flow amplitude and the flow direction. A further discussion about the parametrization of the flow rule can be found in [36].

Once the tensor $\boldsymbol{N}$ is obtained, the single equation remaining to be solved arises from the optimality condition related to the flow amplitude and is analogous to Eq. (24)

$$\mathring{r} + \frac{s\left(r_{n+\alpha}\right)}{\mu_H \Delta t}\left(\frac{\mathring{r}}{\dot{r}_0}\right)^m + \frac{\alpha}{\mu_H\left(m+1\right)}\frac{\mathrm{d}s}{\mathrm{d}r}\left(r_{n+\alpha}\right)\left(\frac{\mathring{r}}{\dot{r}_0}\right)^{m+1} = \frac{\sqrt{2}}{\Delta t}\left\|\mathrm{dev}\left(\boldsymbol{\varepsilon}^{\mathrm{pre}}_{n+1}\right)\right\| \tag{34}$$

A study and discussion on the effects of the algorithmic parameter α over the general solution and convergence properties for J2 elasto-viscoplasticity can be seen in [39]. The special case of a null algorithmic parameter ($\alpha = 0$) renders

$$\mathring{r} + \frac{s\left(r_n\right)}{\mu_H \Delta t}\left(\frac{\mathring{r}}{\dot{r}_0}\right)^m = \frac{\sqrt{2}}{\Delta t}\left\|\mathrm{dev}\left(\boldsymbol{\varepsilon}^{\mathrm{pre}}_{n+1}\right)\right\| \tag{35}$$

Note that when solving for a new state at t_{n+1}, the quantities $\frac{\sqrt{2}}{\Delta t}\left\|\mathrm{dev}\left(\boldsymbol{\varepsilon}^{\mathrm{pre}}_{n+1}\right)\right\|$ and $\frac{s(r_n)}{\mu_H \Delta t}$ are well defined and depend solely on information from the previous state $\mathcal{E}_n$, and thus are constants in this equation. Also, note that the flow resistance curve (s) just needs to be sampled at a given accumulated inelastic strain r_n and not solved as an internal variable, as commonly found in the literature. After solving Eq. (34), the variables $\mathring{r}$ and $\boldsymbol{N}$ (Eq. 32) are used to update states ($\mathcal{E}_n \rightarrow \mathcal{E}_{n+1}$) (Eqs. 29, 30).

Analogously to the continuous time formulation (Eq. 22), the updated first Piola–Kirchhoff $\boldsymbol{P}_{n+1}$ can also be obtained directly from an effective incremental potential [24]

$$\boldsymbol{P}_{n+1} = \frac{\partial \Psi^{\mathrm{eff}}_{\mathrm{inc}}}{\partial \boldsymbol{F}_{n+1}}, \quad \Psi^{\mathrm{eff}}_{\mathrm{inc}}\left(\boldsymbol{F}_{n+1}\right) = \inf_{\substack{\mathring{r} \in \mathbb{R}_+ \\ \boldsymbol{N} \in \mathcal{N}}} \psi\left(\mathcal{E}_{n+1}\right) - \psi\left(\mathcal{E}_n\right) + \Delta t \phi\left(\mathring{\mathcal{E}}; \mathcal{E}_{n+\alpha}\right) \tag{36}$$

Again, due to the particular dependencies of the proposed dissipative potential (Eq. 17), only the Helmholtz free energy contributes to the calculation of the stress tensor

$$\boldsymbol{P}_{n+1} = \frac{\partial \Psi^{\mathrm{eff}}_{\mathrm{inc}}}{\partial \boldsymbol{F}_{n+1}} = \frac{\partial \psi}{\partial \boldsymbol{F}_{n+1}}\left(\mathcal{E}_{n+1}\right) \tag{37}$$

which ends up generating the same relation as Eq. (27) for the updated first Piola–Kirchhoff stress $\boldsymbol{P}_{n+1}$, with all the quantities being evaluated at the updated state $\mathcal{E}_{n+1}$. An overview of the derived constitutive update algorithm is shown in table (Algorithm 1).

Algorithm 1 Constitutive Update Algorithm

Given:

1. A set of material parameters
2. A previous state $\mathcal{E}_n = \left\{\boldsymbol{F}_n, \boldsymbol{F}^{\mathrm{p}}_n, r_n\right\}$ at t_n
3. An updated total deformation gradient $\boldsymbol{F}_{n+1}$ at t_{n+1}

Calculate:

1. The predictor state $\mathcal{E}^{\mathrm{pre}}_{n+1}$ (Eq. 33)
2. The analytical flow direction $\boldsymbol{N}$ (Eq. 32)
3. Solve for the flow amplitude $\mathring{r}$ (Eq. 34)
4. The updated accumulated inelastic strain r_{n+1} (Eq. 29)
5. The updated inelastic deformation gradient $\boldsymbol{F}^{\mathrm{p}}_{n+1}$ (Eq. 30)
6. The updated first Piola–Kirchhoff tensor $\boldsymbol{P}_{n+1}$ (Eq. 37)

End. The state $\mathcal{E}_{n+1} = \left\{\boldsymbol{F}_{n+1}, \boldsymbol{F}^{\mathrm{p}}_{n+1}, r_{n+1}\right\}$ at t_{n+1} is known.

4 Extension to multiple Maxwell branches

The inclusion of multiple rheological branches, such as Kelvin and Maxwell ones, is a common practice described in many textbooks on linear viscoelasticity to improve the predictions of polymers. For instance, several parallel Maxwell branches would allow the description of different relaxation intervals, as shown in Fig. 1.

The current framework, presented in Sect. 3, can be extended to include multiple Maxwell branches within the same context of large strains. Each branch has its own Hencky energy (Eq. 11) and its own dissipation potential (Eq. 17), as well as its own set of state variables $\boldsymbol{F}^{\mathrm{p}}$ e r. When these new potentials are included in the variational principle (Eq. 31), it can be shown that the minimization process leads to a set of uncoupled discrete equations, each one with respect to one particular Maxwell branch, analogously to (Eq. 34).

The effect of including one extra branch will be explored in Sect. 6.2 to address the unloading condition of PMMA.

5 Flow resistance function

As stated in Sect. 2.2.2, one aspect that differs from standard methodologies is the employment of an explicit function for the flow resistance (FR). One can consider the resistance to be constant

$$s\left(r\right) = s_0 \tag{38}$$

rendering, for example, a traditional Perzyna flow rule [24,39]. Moreover, a Newtonian flow could be obtained by assuming a linear dependence on the viscous rate. However, these assumptions are not satisfactory to deal with glassy polymers, as they generally show a complex evolution of the flow mechanisms. A better choice would be a function that accounts for the possibility of a FR transition, ranging from an initial state s_0 to a saturated value s_∞. This is the core idea introduced by Boyce et al. [20]. Indeed, starting from expression (18), the FR evolution is directly obtained by a simple chain rule

$$\dot{s} = \frac{\mathrm{d}s}{\mathrm{d}t} = \frac{\mathrm{d}s}{\mathrm{d}r}\frac{\mathrm{d}r}{\mathrm{d}t} = \frac{\mathrm{d}s}{\mathrm{d}r}\dot{r} \tag{39}$$

This expression has been used as a standard template to tailor the evolution of the flow resistance over the last years. Small changes of notation aid to see that [20] propose the following evolution law in their model

$$\dot{s} = h\left(1 - \frac{s}{s_\infty}\right)\dot{r}, \quad s\left(0\right) = s_0 \tag{40}$$

which is a particular case of (39). Time dependency can then be eliminated from (40) leading to a differential equation relating s and r solely, with solution

$$s\left(r\right) = s_\infty + \left(s_0 - s_\infty\right)e^{-\zeta r} \tag{41}$$

Function (41) captures the essence of the model introduced by Boyce et al. [20]. An even more elaborated evolution is the system proposed by Anand and Gurtin [21], conveniently rewritten below

$$\dot{s} = h\left[1 - \frac{s}{s_\infty\left[1 + b\left(\eta_{cv} - \eta\right)\right]}\right]\dot{r}, \quad s\left(0\right) = s_0 \tag{42}$$

$$\dot{\eta} = g\left(\frac{s}{s_\infty} - 1\right)\dot{r}, \quad \eta\left(0\right) = 0 \tag{43}$$

which depends on a new variable η that measures the free volume within polymeric chains. Analogously to (40), the FR and the free volume evolution rules expressed in (42) and (43) can be recast, arriving to a nonlinear non-homogeneous system of differential equations. Unfortunately, working with this kind of coupled system within the context of implicit finite element schemes is a cumbersome task, and thus an approximation is sought. In principle, Eq. (42) could be linearized with respect to η leading to a non-homogeneous, but linear, system of differential equations with general solution

$$s\left(r\right) = a_0 + a_1 e^{\alpha_1 r} + a_2 e^{\alpha_2 r} \tag{44}$$

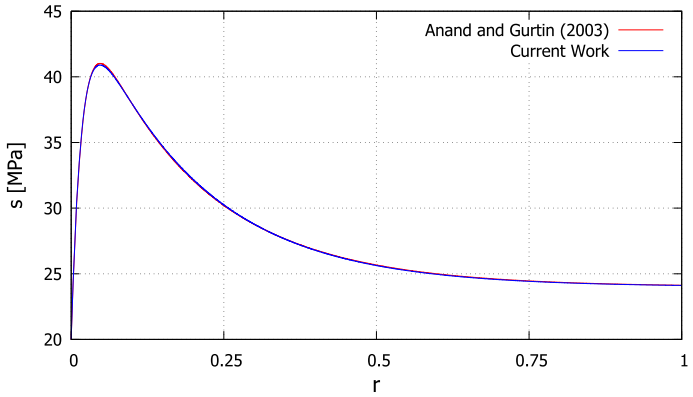

Fig. 2 Flow resistance. Comparison between [21] (Eqs. 42–43) and the current work (Eq. 44)

In order to assess whether the last expression is in fact an approximate solution of the nonlinear system (42–43), both responses are simultaneously plot in the Fig. 2. Clearly, the proposed expression closely follows the original curve and consequently is able to represent the initial grow and subsequent decrement of the flow resistance as a function of r. In addition, the number of controlling material parameters reduces from 6 to 5. Expression (44) then becomes a convenient alternative way to describe the principles introduced by Anand and Gurtin [21] and appropriately represent the strain softening phenomenon. It should be emphasized that, despite previous reasoning, no complete equivalence between both material models is claimed since they differ in their overall rheological representation.

Unfortunately, the biexponential function as represented by (Eq. 44) is not adequate for material parameter identification. Conveniently, the same equation can be rewritten by the use of auxiliary functions

$$s\left(r\right) = s_0 N_0\left(r\right) + s_* N_*\left(r\right) + s_\infty N_\infty\left(r\right) \tag{45}$$

In this way, it becomes possible to directly correlate three characteristic resistances $\{s_0, s_*, s_\infty\}$ with three values of r. The initial resistance s_0 is associated with $r = 0$

$$s\left(0\right) = s_0\,, \tag{46}$$

the ultimate resistance s_∞ to the limit $r \to \infty$

$$\lim_{r\to\infty} s\left(r\right) = s_\infty\,, \tag{47}$$

and an intermediate resistance s_* can be linked to a given convenient value $r = r_* > 0$

$$s\left(r_*\right) = s_* \tag{48}$$

The intermediate pair (r_*, s_*) may be set to be near the peak value, for example. The functions built to match these criteria are explicitly given by

$$N_0\left(r\right) = \frac{e^{-\zeta r_* - \beta r} - e^{-\beta r_* - \zeta r}}{e^{-\zeta r_*} - e^{-\beta r_*}} \tag{49}$$

$$N_*\left(r\right) = \frac{e^{-\zeta r} - e^{-\beta r}}{e^{-\zeta r_*} - e^{-\beta r_*}} \tag{50}$$

$$N_\infty\left(r\right) = 1 - N_0\left(r\right) - N_*\left(r\right) \tag{51}$$

The parameters ζ and β control the overall shape of the function, providing a rapid (or slow) evolution toward s_* and s_∞. It is important to note that functions (44) and (45) exactly match each other, representing the same biexponential evolution of the flow resistance. Thus, it is just a matter of convenience selecting one or another, as the choice does not change the behavior of the constitutive problem. These auxiliary functions are given in Fig. 3 for a given set of parameters (ζ, β, r_*).

As well as other available FR models (in the format of evolution equations) found in the literature [16,22], the biexponential function provides an increased flexibility for the description of the initial behavior of the

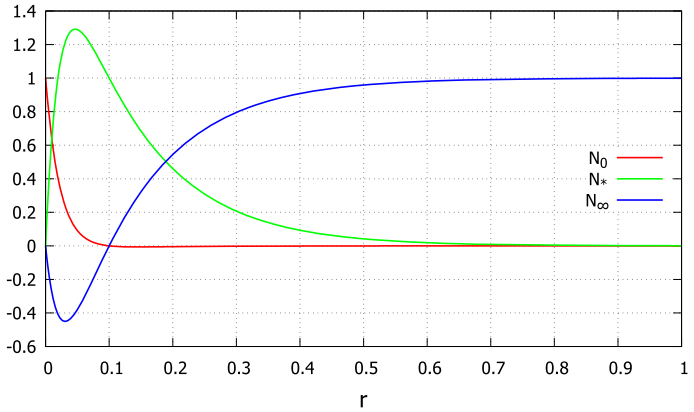

Fig. 3 Example of auxiliary functions $N_0,\ N_*,\ N_\infty$ for $\zeta = 8$, $\beta = 45$ and $r_* = 0.1$

flow resistance. On the other hand, this extra flexibility can be detrimental to the material model by possibly introducing parameters with low overall sensitivity. Guided by these observations, the authors would like to introduce another FR function with a slight incremental improvement to the exponential model, accounting for a possible delayed (although also exponential) evolution

$$s\left(r\right) = s_\infty + \left(s_0 - s_\infty\right) e^{-\zeta \langle r - r_* \rangle_+} \tag{52}$$

The parameter r_* is a characteristic accumulated inelastic strain that triggers the loss of resistance through the ramp function $\langle x \rangle_+ = \left(x + |x|\right)/2$. Evidently, one can still recover the exponential model by manually setting $r_* = 0$, or by obtaining a null fitted r_* parameter.

All three flow resistance functions (the exponential model (Eq. 41), delayed exponential model (Eq. 52) and biexponential model (Eq. 45)) predict a softening saturation value s_∞, attained when the accumulated inelastic strain approaches infinity. One could associate this behavior to a well-known class of saturation models found in plasticity theory, such as the Armstrong–Frederick model. However, it is important to note that the Armstrong–Frederick model accounts for kinematic hardening, yielding a backstress tensor, whereas the model presented here does not.

These flow resistance functions will be employed and evaluated in the next section.

6 Numerical results

The main purpose of this section is to address some numerical experiments with the proposed model in order to verify its capabilities. To completely define the model, the following material parameters are required; the hyperelastic nature of the model is described by μ_H (Hencky Energy, Eq. 11), κ (volumetric energy, Eq. 8), $\{\mu_L, \lambda\}$ (chain locking energy, Eq. 9); and the dissipative nature of the model is partially described by the exponent m (dissipative potential, Eq. 17). The remaining of the dissipative potential makes use of a FR function $s\left(r\right)$, which requires one of the following sets depending on the model chosen to describe it: $\{s_0, s_\infty, \zeta\}$ for an exponential evolution (Eq. 41),$\{s_0, s_\infty, \zeta, r_*\}$ for a delayed exponential evolution (Eq. 52); or $\{s_0, s_*, s_\infty, \zeta, \beta\}$ for a biexponential evolution (45). Note that $\dot{r}_0$ in Eq. (17) is just an unitary parameter to ensure that units are compatible.

6.1 PETG—poly(ethylene terephthalate)–glycol

Experimental data were extracted from the literature to verify if the proposed model is able to capture the essence of the behavior of polymers in real tests. Even though it is provided later on, the authors do not claim to have found any definitive set of material parameters to be used in real applications, due to the small number of experiments used to calibrate the model. Special focus is given to issues like strain softening, evolution of flow resistance, and the strain rate dependence. It is tacitly assumed that all experimental results already represent the intrinsic material point behavior, and thus any other non-local or structural effect is neglected.

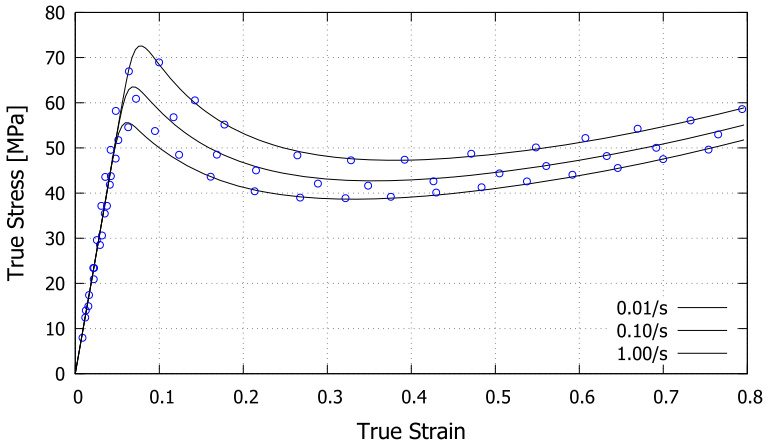

Fig. 4 PETG: experimental results from Dupaix and Boyce [57] (markers) and prediction using the exponential flow resistance model (Eq. 41)

A set of experimental results was extracted from the work of Dupaix and Boyce [57], where uniaxial and plane strain compression experiments were performed on poly(ethylene terephthalate) (PET) and poly(ethylene terephthalate)–glycol (PETG) at different temperatures and strain rates. Among these, the uniaxial compression tests for PETG at the temperature of 25° C and strain rates $\{0.01,\ 0.10,\ 1.00\}$ $[1/s]$ were selected. The constitutive model was fitted to this set of experimental data three times, each one assessing one particular flow resistance model. Following Dupaix [58], the Poisson's ratio was assumed to be 0.33. The resulting compression behaviors can be seen in the Figs. 4(Exponential FR), 5(Delayed Exponential FR) and 6(Biexponential FR), where the markers refer to the experimental data and the solid lines to the model prediction. One can notice that, independently of the flow resistance model adopted, all three functions provide qualitatively the same overall results and are able to capture the strain softening behavior.

The fitted FR functions associated with this material are displayed in Fig. 7. It becomes clear that the main difference among the three tested FR models is the flexibility for describing the initial flow resistance evolution. Noticing that all these FR models share the same asymptotic loss of resistance, the exponential model only allows for an immediate loss, whereas the delayed exponential and the biexponential can either keep or increase the initial resistance. This initial excessive rigidity showed by the exponential model is then propagated toward the ultimate resistance ($r \to \infty$) to account for "error compensation", and hence the possible inferior predictive capability. The authors would like to point that drawing one definitive statement for rejecting one model against the other is not reasonable from just one set of experiments. Nonetheless, as a highlight, note that this intuitive aspect of interpreting and visualizing a flow resistance curve allows and creates a more practical environment for constitutive modeling, instead of dealing with evolution laws in the format of differential equations.

The set of fitted parameters are given in Table 1. As the hyperelastic nature of the whole material model is the same for all tested FR functions, as well as the power-law-like dissipative behavior, the specific FR parameters were split into a separated table for a better insight of the different aspects provided by each one. The parameters s_0, s_∞ and s_* (the last one available only in the biexponential model) are self-explanatory, as they represent the flow resistance sampled at targeted locations, $r = 0$, $r \to \infty$ and $r = r_*$ respectively. The parameter ζ controls the resistance decay toward s_∞, and for the biexponential model β has a mixed influence over the initial resistance growth and peak location. In the delayed exponential model, r_* sets the critical inelastic strain at which the material starts to experience resistance loss, in this particular case being of around 6.1%. That is, the material would behave as a standard constant "viscosity" model up to an accumulated inelastic strain of 6.1%, and afterward would start to lose resistance. At this stage, the entropic mechanisms would dictate how the material point recovers its stability, as predicted by (9).

6.2 PMMA—poly(methyl methacrylate)

Experimental results for PMMA can be found in the work of Ames et al. [13], where uniaxial compression load–unload experiments were performed at different temperatures and strain rates. The uniaxial compression

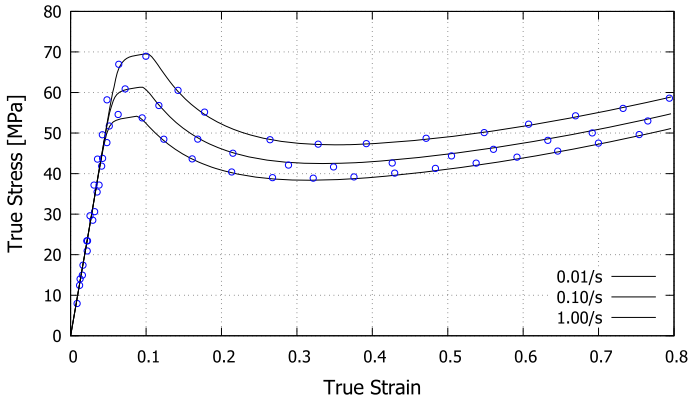

Fig. 5 PETG: experimental results from Dupaix and Boyce [57] (markers) and prediction using the delayed exponential flow resistance model (Eq. 52)

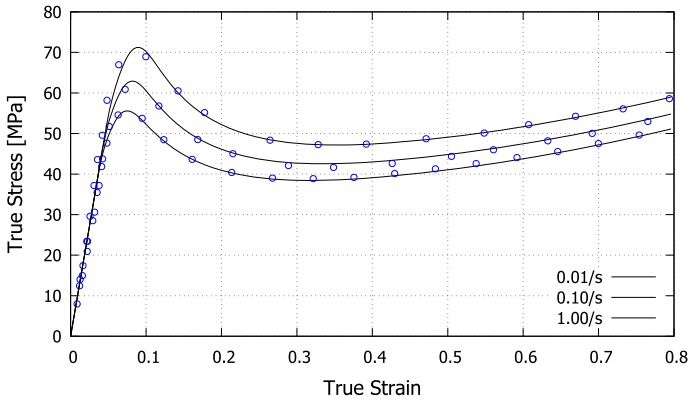

Fig. 6 PETG: experimental results from Dupaix and Boyce [57] (markers) and prediction using the biexponential flow resistance model (Eq. 44)

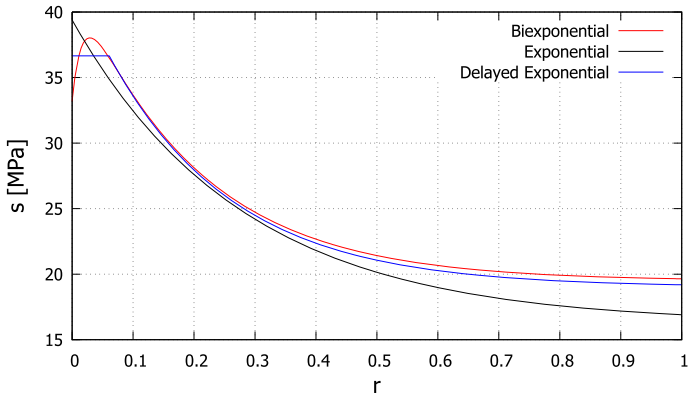

Fig. 7 PETG: resulting fitted flow resistance functions for each model

tests for PMMA at the temperature of 100° C and strain rates $\{0.0003, 0.001, 0.01, 0.1\}$ $[1/s]$ were selected. In this case, the unload history may not be properly captured employing just one Maxwell branch. Figure 8 aims at illustrating this fact, where it is evident that different strain rates render significantly different unload curves.

To address this behavior, two Maxwell branches were considered. The first one uses a biexponential flow resistance model (Eq. 44) and the second one is assumed to have constant resistance (Eq. 38). Table 2 contains the fitted parameters and Fig. 9 shows the predictions employing these two branches. Clearly, the adoption of

Table 1 PETG: Fitted parameters

(a) Shared parameters				
FR model	μ_H (MPa)	μ_L (MPa)	λ	m
Exponential	384.4	12.2	11.56	0.0577
Delayed exponential	391.2	9.92	9.579	0.0545
Biexponential	396.4	9.26	8.059	0.0537

(b) Flow resistance function parameters						
FR model	s_0 (MPa)	s_∞ (MPa)	s_* (MPa)	r_*	ζ	β
Exponential	39.4	16.2	–	–	3.563	–
Delayed exponential	36.6	19.0	–	0.0609	4.898	–
Biexponential	33.2	19.5	33.7	0.1000(1)	4.982	60.24

(1) Instead of a material property, this is a constant that describes the accumulated inelastic strain at which the material property s_* is being evaluated

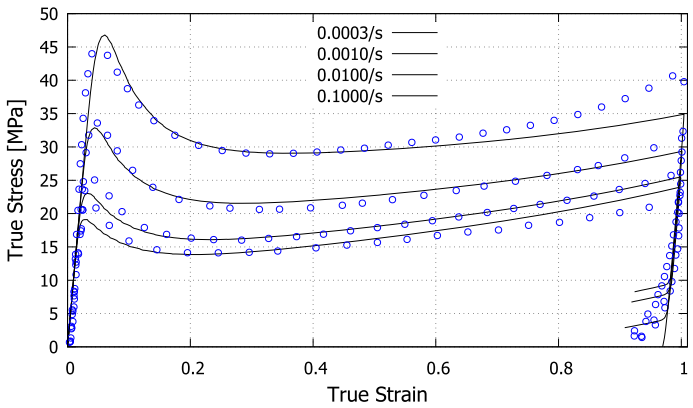

Fig. 8 PMMA: experimental results from [13] (markers) and predictions using one Maxwell branch with a biexponential flow resistance model (Eq. 44)

Table 2 PMMA: Fitted parameters with two Maxwell branches

(a) Parameters for the first Maxwell branch. Biexponential flow resistance model							
μ_H (MPa)	m	s_0 (MPa)	s_∞ (MPa)	s_* (MPa)	β	ζ	r_*
349.1	0.165	30.67	8.004	17.598	1.393	6.020	0.100

(b) Parameters for the second Maxwell branch. Constant flow resistance model		
μ_H (MPa)	m	s_0 (MPa)
58.676	0.129	13.670

(c) Volumetric and Gent branches		
κ (GPa)	μ_L (MPa)	λ
1.071	2.985	64.68

Temperature 100°C

another branch improves the unloading behavior by providing extra flexibility and making it less sensitive to different strain rates.

6.3 Convergence and algorithmic parameter

Being a numerical framework and based on discrete time approximations, it becomes important to verify how time intervals influence the solution concerning stress convergence. Moreover, motivated by the simplification

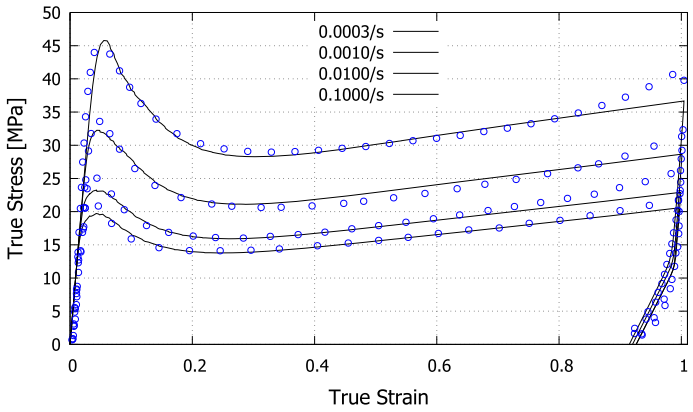

Fig. 9 PMMA: experimental results from [13] (markers) and predictions using two Maxwell branches. First branch employs a biexponential flow resistance model (Eq. 44) and the second one has a constant resistance (Eq. 38). Both branches follow a power-law flow rule (Eq. 17)

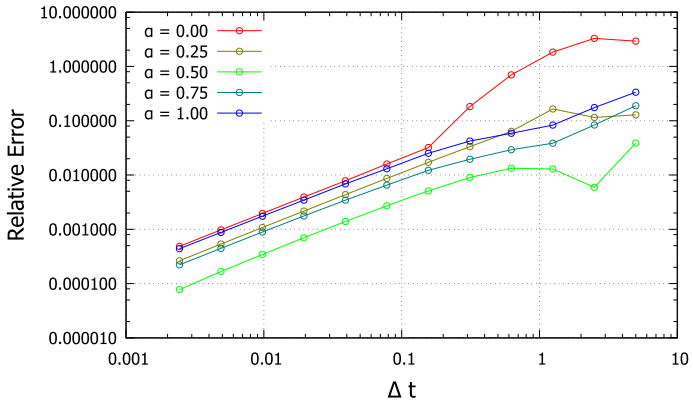

Fig. 10 Convergence assessment. Maximum relative error

provided by the algorithmic parameter α [cf. (34) and (35)], one may wonder what are the observed effects of a particular choice for α. To this end, different simulations were performed, each one having its own time interval Δt and algorithmic parameter α (Eq. 34). A solution used as reference was generated using a large number of time divisions, namely $\mathcal{O}\left(10^5\right)$, thus resulting in a small time increment. For each pair $(\Delta t, \alpha)$ the numerical experiment consisted of a simple tensile test with constant strain rate, and the maximum relative error in stress (e)

$$e\left(\Delta t, \alpha\right) = \max_{t \in [t_0, t_f]} \frac{\left\| \boldsymbol{\sigma} - \boldsymbol{\sigma}_{ref} \right\|}{\left\| \boldsymbol{\sigma}_{ref} \right\|} \tag{53}$$

was computed and registered. Figure 10 gathers all these results. As the time interval becomes smaller, so does the maximum relative error. Independently of the algorithmic parameter α, a linear convergence could be observed, which matches the observations of Brassart and Stainier [39] for small strain J2 plasticity, and is consistent with a backward-Euler scheme. One can see that, for these experiments, a parameter of $\alpha = 0.5$ performed the best, although as pointed out by Brassart and Stainier [39] there may actually exist one optimal α for each set of material parameters used within the model. Regarding the relative error itself, the parameters $\alpha = 0$ and $\alpha = 1$ performed virtually the same, but Eq. (35) to be solved for each time increment is simpler in the former case. This fact also renders a competitive alternative against $\alpha = 0.5$.

6.4 FEM framework

The proposed viscoelastic model was implemented inside a standard *quasi-static* FEM framework and a tensile test of a 3D specimen was performed. The geometry was generated according to the ASTM D638 standard for

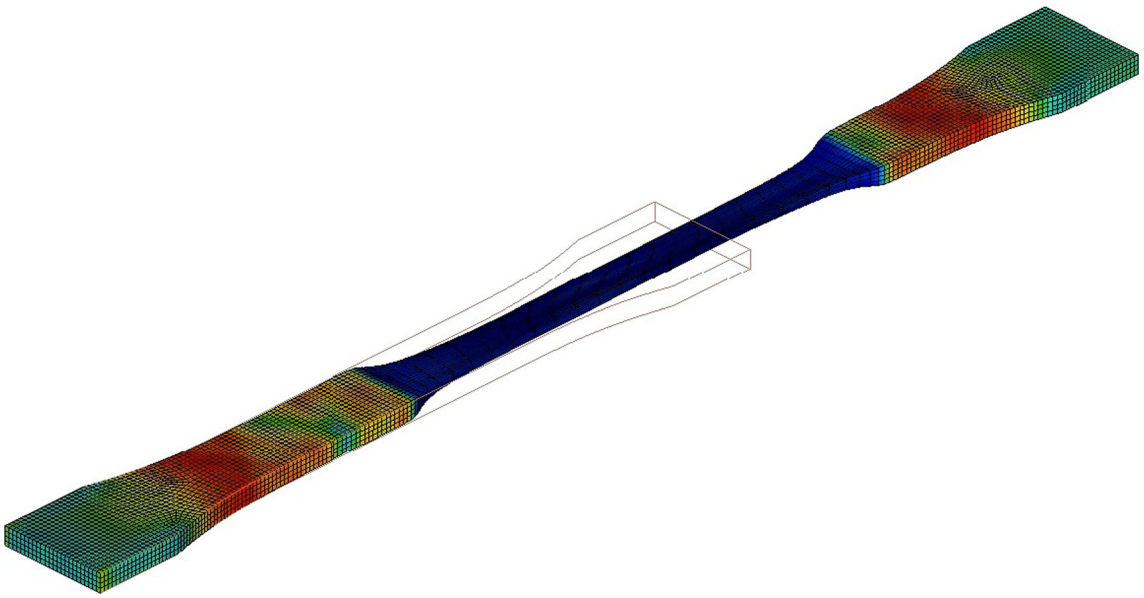

Fig. 11 Three-dimensional view of the tensile test of a standard specimen. Color map corresponds to the flow resistance and the wireframe edges correspond to the undeformed geometry (color figure online)

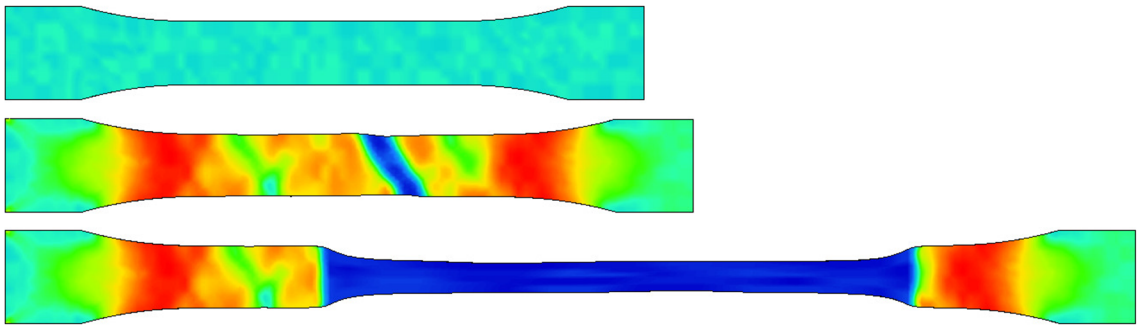

Fig. 12 Tensile test of a standard specimen. Color map corresponds to the flow resistance at $t = 0s$, $t = 10s$ and $t = 100s$ (color figure online)

a Type I specimen. A prescribed displacement rate of $u = 1\,mm/s$ was set at the extremity of the specimen. The test was conducted for the fitted PETG (Sect. 6.1) using the biexponential flow resistance model (Eq. 45).

From the experimental point of view, it is extremely difficult to ensure all symmetries (material, geometry and boundary conditions). Thus, it is common practice to consider just a fraction of the geometry and endorse it with appropriate symmetry boundary conditions. To ensure a symmetric physically reasonable response, one could induce macroscopic yielding by artificially moving some nodes and causing a stress concentration at the (symmetric) axial boundary. Even with this practice in hand, some artificial patterns may arise when rebuilding the solution field over the full geometry. Differently, the numerical tensile test performed here was conducted using the entire geometry of the specimen and no symmetry boundary conditions were applied. One more practical and natural way of verifying the macroscopic yielding is to admit that the material is heterogeneous. To this aim, the material properties were allowed to have a variability within a $\pm 1\%$ range, so each integration point would have its own set of properties (Fig. 12).

Figure 11 gathers three time instants from this numerical experiment: the initial state ($t = 0s$); the first evidence of macroscopic yielding (approximately $t = 10s$); the end of the analysis ($t = 100s$). The color map ranges from blue to red and represents the current flow resistance value. One can note the randomized properties through the dispersion of the initial FR shown for $t = 0$. The second snapshot reveals multiple regions that lose resistance simultaneously, and the least resistant one will end up governing the softening behavior and triggering the necking. The third snapshot shows that, even after a long propagation, some regions keep their FR value constant until their cross section is engaged. Figure 13 reveals the overall force at the extremity of

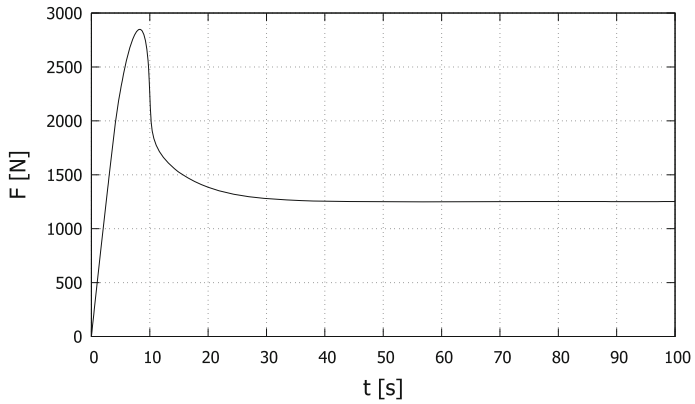

Fig. 13 Force evolution

the specimen as a global result of such a resistance loss, and is compatible with general observed experimental data.

From the numerical point of view, solving only one scalar equation (Eq. 34 or the special case Eq. 35) at each Gauss point revealed to be less time consuming and could reduce coding complexity.

7 Conclusions

The main result brought by the present work is an alternative formalism, set in variational statements, that captures the core of a widely used class of models for glassy polymers. In these models, the inelastic behavior is based on the solution of (eventually coupled) differential equations that account for the evolution of an internal variable called flow resistance. It was shown that the flow resistance can be recast in a simpler framework in which it becomes dependent on an accumulated measure of the inelastic strain. Within this strategy, the flow resistance can be seen as a mechanical property dependent solely on the current state. Three different flow resistance models were discussed and tested.

In addition, the simplicity of the proposition allows its inclusion in most classical thermodynamically consistent constitutive approaches, well suited for the use of implicit finite element codes. Particularly, the adopted variational framework reduced the local constitutive problem to the solution of a single nonlinear scalar equation, emulating the simplest case of viscoelastic models. The extension to multiple Maxwell branches was discussed, and it was shown to be able to capture the unloading behavior of PMMA.

Numerical assessments showed an excellent agreement with compression experiments, and a monotonic linear stress convergence could be observed for small time steps. A FEM example was used to verify a tensile test for a 3D specimen having a heterogeneous material distribution.

Clearly, further dependencies have to be accounted for in order to turn this approach able to reproduce more general thermomechanical behaviors observed in these materials. Temperature coupling and pressure flow dependence are among the most classical ones that could be included within the same variational approach, following similar ideas of Yang et al. [26].

Acknowledgements Eduardo A. Fancello and Jan-Michel C. Farias thank the financial support provided by CNPq-Brazil (Grant 313146/2017-9).

Compliance with ethical standards

Conflict of interest The authors declare that there is no conflict of interest.

References

1. Kurtz, S.M., Devine, J.N.: PEEK biomaterials in trauma, orthopedic, and spinal implants. Biomaterials **28**, 4845–4869 (2007)
2. Smith, K.E., Temenoff, J.S., Gall, K.: On the toughness of photopolymerizable (meth)acrylate networks for biomedical applications. J. Appl. Polym. Sci. **114**, 2711–2722 (2009)

3. Ulery, B.D., Nair, L.S., Laurencin, C.T.: Biomedical applications of biodegradable polymers. J. Polym. Sci. B **49**, 832–864 (2011)
4. Miller, A.T., Safranski, D.L., Smith, K.E., Guldberg, R.E., Gall, K.: Compressive cyclic ratcheting and fatigue of synthetic, soft biomedical polymers in solution. J. Mech. Behav. Biomed. Mater. **54**, 268–282 (2016)
5. Spitzig, W.A., Richmond, O.: Effect of hydrostatic pressure on the deformation behavior of polyethylene and polycarbonate in tension and in compression. Polym. Eng. Sci. **19**, 1129–1139 (1979)
6. G'Sell, C., Hiver, J.M., Dahoun, A., Souahi, A.: Video-controlled tensile testing of polymers and metals beyond the necking point. J. Mater. Sci. **27**, 5031–5039 (1992)
7. Arruda, E.M., Boyce, M.C., Jayachandran, R.: Effects of strain rate, temperature and thermomechanical coupling on the finite strain deformation of glassy polymers. Mech. Mater. **19**, 193–212 (1995)
8. Khan, A., Zhang, H.: Finite deformation of a polymer: experiments and modeling. Int. J. Plast. **17**, 1167–1188 (2001)
9. Nakafuku, C., Takehisa, S.Y.: Glass transition and mechanical properties of PLLA and PDLLA-PGA copolymer blends. J. Appl. Polym. Sci. **93**, 2164–2173 (2004)
10. Khan, A.S., Lopez-Pamies, O., Kazmi, R.: Thermo-mechanical large deformation response and constitutive modeling of viscoelastic polymers over a wide range of strain rates and temperatures. Int. J. Plast. **22**, 581–601 (2006)
11. Richeton, J., Ahzi, S., Vecchio, K.S., Jiang, F.C., Adharapurapu, R.R.: Influence of temperature and strain rate on the mechanical behavior of three amorphous polymers: characterization and modeling of the compressive yield stress. Int. J. Solids Struct. **43**, 2318–2335 (2006)
12. Dreistadt, C., Bonnet, A.S., Chevrier, P., Lipinski, P.: Experimental study of the polycarbonate behaviour during complex loadings and comparison with the Boyce, Parks and Argon model predictions. Mater. Des. **30**, 3126–3140 (2009)
13. Ames, N.M., Srivastava, V., Chester, S.A., Anand, L.: A thermo-mechanically coupled theory for large deformations of amorphous polymers. Part II: applications. Int. J. Plast. **25**, 1495–1539 (2009)
14. Wright, D.D., Lautenschlager, E.P., Gilbert, J.L.: The effect of processing conditions on the properties of poly(methyl methacrylate) fibers. J. Biomed. Mater. Res. **63**, 152–160 (2002)
15. Viana, J.C., Alves, N.M., Mano, J.F.: Morphology and mechanical properties of injection molded poly(ethylene terephthalate). Polym. Eng. Sci. **44**, 2174–2184 (2004)
16. Holopainen, S.: Modeling of the mechanical behavior of amorphous glassy polymers under variable loadings and comparison with state-of-the-art model predictions. Mech. Mater. **66**, 35–58 (2013)
17. Gudimetla, M.R., Doghri, I.: A finite strain thermodynamically-based constitutive framework coupling viscoelasticity and viscoplasticity with application to glassy polymers. Int. J. Plast. **98**, 197–216 (2017)
18. Haward, R.N., Thackray, G.: The use of a mathematical model to describe isothermal stress–strain curves in glassy thermoplastics. Proc. R. Soc. Lond. A **302**, 453–472 (1968)
19. Bagepalli, B.S.: Finite strain elastic-plastic deformation of glassy polymers. Ph.D. thesis, Massachusetts Institute of Technology (1984)
20. Boyce, M.C., Parks, D.M., Argon, A.S.: Large inelastic deformation of glassy polymers. Part I: rate dependent constitutive model. Mech. Mater. **7**, 15–33 (1988)
21. Anand, L., Gurtin, M.E.: A theory of amorphous solids undergoing large deformations, with application to polymeric glasses. Int. J. Solids Struct. **40**, 1465–1487 (2003)
22. Poulain, X., Benzerga, A.A., Goldberg, R.K.: Finite-strain elasto-viscoplastic behavior of an epoxy resin: experiments and modeling in the glassy regime. Int. J. Plast. **62**, 138–161 (2014)
23. Srivastava, V., Chester, S.A., Ames, N.M., Anand, L.: A thermo-mechanically-coupled large-deformation theory for amorphous polymers in a temperature range which spans their glass transition. Int. J. Plast. **26**, 1138–1182 (2010)
24. Ortiz, M., Stainier, L.: The variational formulation of viscoplastic constitutive updates. Comput. Methods Appl. Mech. Eng. **171**, 419–44 (1999)
25. Radovitzky, R., Ortiz, M.: Error estimation and adaptive meshing in strongly nonlinear dynamic problems. Comput. Methods Appl. Mech. Eng. **172**, 203–240 (1999)
26. Yang, Q., Stainier, L., Ortiz, M.: A variational formulation of the coupled thermo-mechanical boundary-value problem for general dissipative solids. J. Mech. Phys. Solids **54**, 401–424 (2006)
27. Fancello, E.A., Ponthot, J.-P., Stainier, L.: A variational formulation of constitutive models and updates in non-linear finite viscoelasticity. Int. J. Numer. Methods Eng. **65**, 1831–1864 (2006)
28. Mosler, J., Bruhns, O.T.: Towards variational constitutive updates for non-associative plasticity models at finite strain: models based on a volumetric-deviatoric split. Int. J. Solids Struct. **46**, 1676–1684 (2009)
29. Mosler, J.: Variationally consistent modeling of finite strain plasticity theory with non-linear kinematic hardening. Comput. Methods Appl. Mech. Eng. **199**, 2753–2764 (2010)
30. Kintzel, O., Mosler, J.: An incremental minimization principle suitable for the analysis of low cycle fatigue in metals: a coupled ductile-brittle damage model. Comput. Methods Appl. Mech. Eng. **200**(45–46), 3127–3138 (2011)
31. El Sayed, T., Mota, A., Fraternali, F., Ortiz, M.: A variational constitutive model for soft biological tissues. J. Biomech. **41**(7), 1458–66 (2008)
32. Vassoler, J.M., Reips, L., Fancello, E.A.: A variational framework for fiber-reinforced viscoelastic soft tissues. Int. J. Numer. Methods Eng. **89**, 1691–1706 (2012)
33. Stainier, L., Ortiz, M.: Study and validation of a variational theory of thermo mechanical coupling in finite visco-plasticity. Int. J. Solids Struct. **47**, 705–715 (2010)
34. Miehe, C.: A multi-field incremental variational framework for gradient-extended standard dissipative solids. J. Mech. Phys. Solids **59**, 898–923 (2011)
35. Stainier, L.: Consistent incremental approximation of dissipation pseudo-potentials in the variational formulation of thermo-mechanical constitutive updates. Mech. Res. Commun. **38**, 315–319 (2011)
36. Bleier, N., Mosler, J.: Efficient variational constitutive updates by means of a novel parameterization of the flow rule. Int. J. Numer. Methods Eng. **89**, 1120–1143 (2012)

37. Brassart, L., Stainier, L., Doghri, I., Delannay, L.: A variational formulation for the incremental homogenization of elasto-plastic composites. J. Mech. Phys. Solids **59**, 2455–2475 (2011)
38. Brassart, L., Stainier, L., Doghri, I., Delannay, L.: Homogenization of elasto-(visco) plastic composites based on an incremental variational principle. Int. J. Plast. **36**, 86–112 (2012)
39. Brassart, L., Stainier, L.: On convergence properties of variational constitutive updates for elasto-visco-plasticity. GAMM-Mitteilungen **35**, 26–42 (2012)
40. Bartels, A., Bartel, T., Canadija, M., Mosler, J.: On the thermomechanical coupling in dissipative materials: a variational approach for generalized standard materials. J. Mech. Phys. Solids **82**, 218–234 (2015)
41. Junker, P., Hackl, K.: A condensed variational model for thermo-mechanically coupled phase transformations in polycrystalline shape memory alloys. J. Mech. Behav. Mater. **22**, 111–118 (2013)
42. Lee, E.H.: Elastic plastic deformation at finite strain. ASME J. Appl. Mech. **36**, 1–6 (1969)
43. Anand, L., Ames, N.M.: On modeling the micro-indentation response of an amorphous polymer. Int. J. Plast. **22**, 1123–1170 (2006)
44. Simo, J.C., Taylor, R.L., Pister, K.S.: Variational and projection methods for the volume constraint in finite deformation elasto-plasticity. Comput. Methods Appl. Mech. Eng. **51**, 177–208 (1985)
45. Arruda, E.M., Boyce, M.C.: A three-dimensional constitutive model for the large stretch behavior of rubber elastic materials. J. Mech. Phys. Solids **41**, 389–412 (1993)
46. Gent, A.N.: A new constitutive relation for rubber. Rubber Chem. Technol. **69**(1), 59–61 (1996)
47. Ziegler, H.: An Introduction to Thermomechanics. Elsevier, Amsterdam (1977)
48. Hill, R.: A general theory of uniqueness and stability in elastic-plastic solids. J. Mech. Phys. Solids **6**, 236–249 (1958)
49. Ceradini, G.: A maximum principle for the analysis of elastic–plastic systems. Meccanica **1**, 77–82 (1966)
50. Maier, G.: Quadratic programming and theory of elastic-perfectly plastic structures. Meccanica **3**, 236–249 (1968)
51. Capurso, M., Maier, G.: Incremental elastoplastic analysis and quadratic optimization. Meccanica **5**, 107–116 (1970)
52. Pereira, N.Z., Feijoo, R.A.: On kinematical minimum principles for rates and increments in plasticity. Meccanica **21**, 23–29 (1986)
53. Martin, J.B., Reddy, B.D., Griffin, T.B., Bird, W.W.: Applications of mathematical programming concepts to incremental elastic–plastic analysis. Eng. Struct. **9**, 171–176 (1987)
54. Mosler, J., Ortiz, M.: Variational h-adaption in finite deformation elasticity and plasticity. Int. J. Numer. Methods Eng. **72**, 505–523 (2007)
55. Mosler, J., Ortiz, M.: An error-estimate-free and remapping-free variational mesh refinement and coarsening method for dissipative solids at finite strains. Int. J. Numer. Methods Eng. **77**, 437–450 (2009)
56. Weber, G., Anand, L.: Finite deformation constitutive equations and a time integration procedure for isotropic, hyperelastic-viscoplastic solids. Comput. Methods Appl. Mech. Eng. **79**, 173–202 (1990)
57. Dupaix, R.B., Boyce, M.C.: Finite strain behavior of poly(ethylene terephthalate) PET and poly(ethylene terephthalate)-glycol PETG. Polymer **46**, 4827–4838 (2005)
58. Dupaix, R.B.: Temperature and rate dependent finite strain behavior of poly(ethylene terephthalate) and poly(ethylene terephthalate)-glycol above the glass transition temperature. Ph.D. thesis, MIT (2003)